MICHIGAN STATE UNIVERSITY

CYCLOTRON LABORATORY

FINAL DESIGN OF THE K800 MAGNETIC FIELD

G. BELLOMO, H.G. BLOSSER, E. FABRICI, D. JOHNSON, F. G. RESMINI

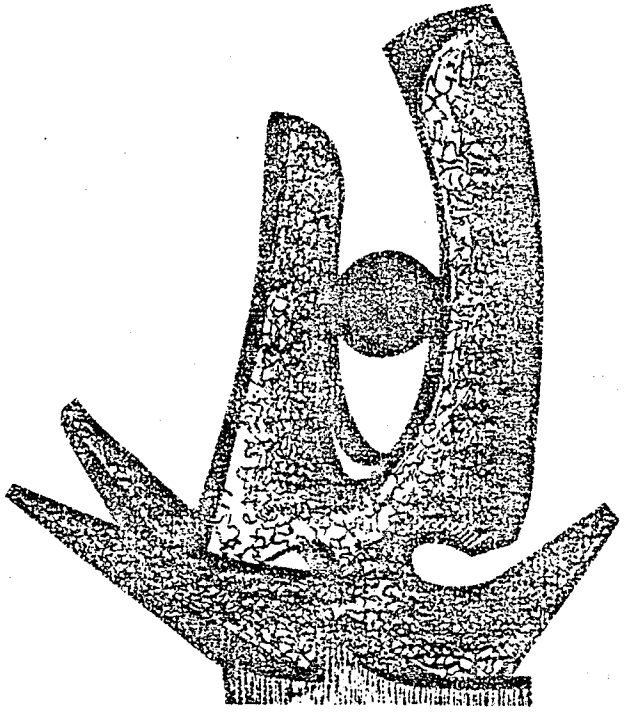

JUNE 1981

MSUCP-35

MSUCP-35
March 1981

FINAL DESIGN OF THE K800 MAGNETIC FIELD

G. Bellomo, H.G. Blosser, E. Fabrici, D. Johnson, F.G. Resmini

Michigan State University, East Lansing, Michigan 48824

FINAL DESIGN OF THE K800 MAGNETIC FIELD

G. Bellomo, H.G. Blosser, E. Fabrici, D. Johnson, F.G. Resmini

Introduction

The status of the magnetic field design for the K800 cyclotron at MSU was last described in the report MSUCP-29,[1] issued in June 1980. At that time a few aspects of the design, mostly concerning the pole tip geometry, minimum hill gap, etc. were still left open to further optimization. Substantial progress has been made since then and the configuration now obtained looks satisfactory enough so as to allow the "freezing" of practically every important parameter.

As a consequence of this further study, many aspects of the finalized geometry are significantly different from those outlined in the Conceptual Design Report (MSUCL-282)[2] and in ref. (3), with implications on magnetic field properties, beam dynamics and extraction. Instead, the injection[4] of beams from the K500 has not been affected by said modifications.

It is the purpose of this paper to review in detail the finalized design of the K800 and the rationale for the choices which have been made, together with their implications on the machine performance.

1. Review of the K800 Characteristics

For the sake of completeness, it is appropriate to briefly review the overall machine characteristics. As well known, the K800 is mainly intended as a booster for the K500 cyclotron, now near completion, although operation with an internal ion source is also anticipated. The energy in MeV/n vs the mass number is shown in Fig. 1, where lines corresponding to constant charge states of beams from the K500 are also drawn. The K800 will

operate mostly with harmonic numbers 1 or 2, as shown at the right of Fig. 1, the R.F. range being between 9 and 32 MHz. The energies of both the K800 and K500 cyclotron are presented in Fig. 2 as a function of the R.F. frequency, for the different harmonic modes possible in coupled operation.

The final parameters of the K800 cyclotron are listed in Table I. The main differences with respect to the Conceptual Design Report (hereafter referred to as CDR) are:

- the increase in pole radius from 41" to 42",
- the increase in the hill gap from 2.5" to 3",
- the increase in the hill width, at outer radii, from 46° to 51°.

The rationale for these choices will be discussed thoroughly in Sec. 3. Here we only need to mention that the 1" pole radius increase has not brought about a corresponding increase in the yoke dimensions. In fact the thickness of the inner vacuum tank wall has been decreased from 2" (as it was originally planned, and as it is in the K500) to 1". The same .25" clearance has been maintained between the pole and the tank wall, as apparent from Fig. 3. A median plane view of the machine, as presently designed, is shown in Fig. 4. Other aspects of the yoke design are very similar to the CDR proposal and need not be discussed in detail here.

The operating diagram of the machine in the (B_o, Z/A) plane is shown in Fig. 5, where the boundaries given by the bending and focusing limits and the $\nu_R + 2\nu_Z = 3$ resonance are indicated. The injection limit in the 7:2 mode, and the h = 2 R.F. limit are the other boundaries of the gray area, i.e. the effective operating

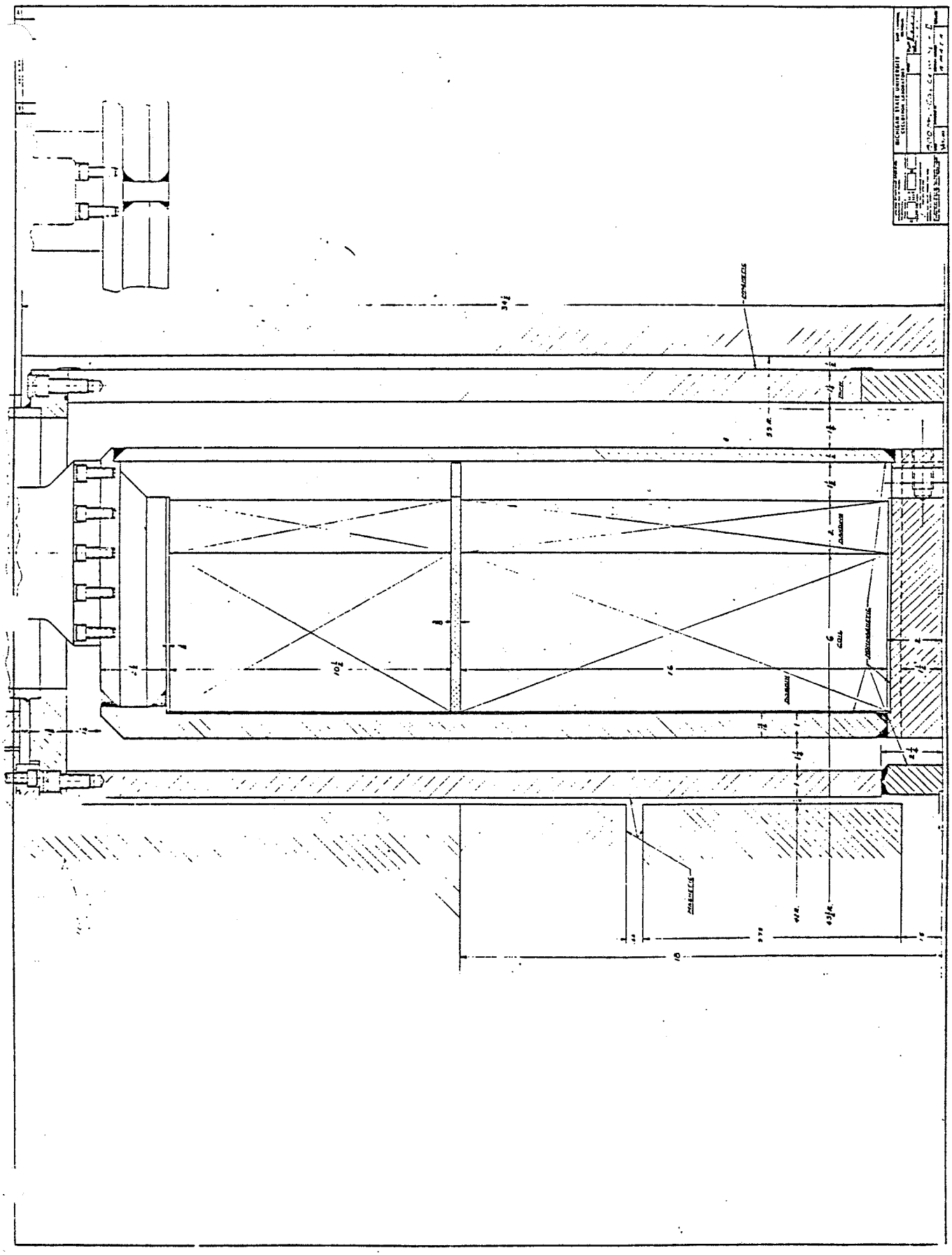

Fig. 3. Cross section of the K800, showing the outer pole region, cryostat and main coils.

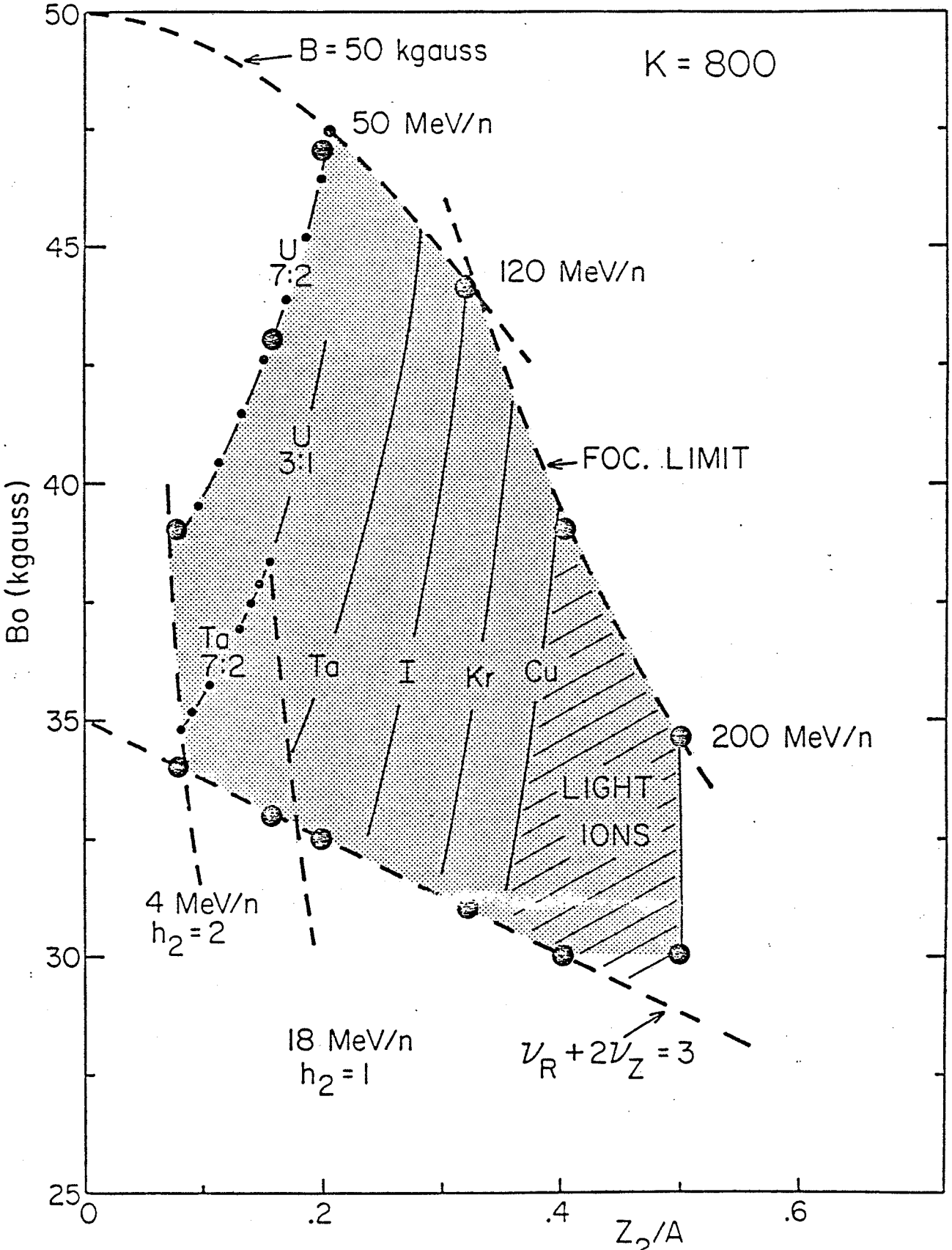

Fig. 5. Operating diagram of the K800 in the (B_o, Z/A) plane. Shown are focusing and bending limits and the low field limit due to the $\nu_R + 2\nu_Z = 3$ resonance. Dots indicate the 12 representative ions chosen to investigate equilibrium orbit properties, etc.

diagram of the K800 when acting as a booster. Some constant energy/nucleon lines, labelled in MeV/n,are plotted with respect to the operating diagram in Fig. 6. This has not changed at all from the CDR and therefore we refer to the latter for more details.

The study presented in this report has been carried out on the basis of twelve ions chosen as representative ones on the operating diagram contours. The field trimming, equilibrium orbit properties, etc. have been investigated for all of them, in order not to leave unknowns in the assessment of the machine performance.

2. Main Coil Design

2.1 General Features

It may be worth recalling that in the CDR only the geometrical characteristics of the main coils had been presented, while several aspects remained open. Progress made since then has allowed the definition of the coils in almost every detail, namely:

- final geometry
- choice of the conductor
- evaluation of forces and stresses

The coil parameters are listed in Table II. The main variation is the increase of the minimum coil distance from the median plane, from 1.5" (as suggested in CDR and as it is in the K500) to 2", as shown in Fig. 3. This increase does not make any worse the magnetic field produced by the coils,presented for both sections in Fig. 7. On the other hand, it allows considerably more axial space for the insertion of the various extraction elements, especially the magnetic channels, and has therefore been selected.

TABLE I. MAIN K800 PARAMETERS

Pole radius	:	42"
Sectors	:	3, 46° wide, flaring to 51° wide between R=37.15" and R=40.2"
Spiral constant	:	1/13 rad/inch (approx)
Minimum hill gap	:	3"
Maximum valley gap	:	36"
Min-max operating average field	:	30-50 kgauss
Yoke height	:	115"
Yoke inner and outer diameters	:	118" - 175"
R.F. frequency range	:	9-32 MHz
Harmonic operating modes	:	1st, 2nd
Peak dee voltage	:	200 kV
No of trim coils	:	22
Max current in any trim coil	:	400 A
Max total trim coil power	:	70 kW
K at 50 kgauss	:	1200
$K_{Focusing}$	:	400

The total coil height has been kept at 26.5" and the two section splitting of the coil is also unchanged, with the section closer to the median plane being 60% of the total as indicated in Table II.

As discussed at some length in the CDR, independent excitation of the two sections allows proper fitting of the isochronous field for all different ions and center field values. The resulting operating diagram of the machine in terms of the current densities J_α and J_β is presented in Fig. 8, all details being given in a straightforward way on the figure itself. As apparent from the

figure, and already anticipated in the CDR, the current J_β (section farther away from the median plane) must go to a negative value with respect to J_α for many of the most relativistic ions, i.e. for Z/A from 0.3 to .5 and for the energies close to the focusing limit.

On this basis we have chosen two limiting cases in order to investigate the forces and the stresses on the coils,as discussed later:

- the first at $J_\alpha = J_\beta = 3500$ A/cm^2, which is outside the actual operating diagram of the machine (at least in the booster option) but is nevertheless a safe upper limit.

- the second at $J_\alpha = 3500$ A/cm^2, $J_\beta = -1500$ A/cm^2, which is close to the excitation needed for 200 MeV/n of fully stripped light ions.

The conductor choice has been dictated mainly by the need to keep the coils inductances within reasonable limits. We have selected for the current a maximum nominal value of 1000 A, i.e. somewhat higher than the one (700 A) for the K500. Accordingly, and as listed in Table II, the overall conductor, which is of the monolithic type, shall have dimensions of .207" x .15", with an overall copper to superconductor ratio of 25:1. The superconductor, to be inserted in a U-shaped slot in the copper of dimensions .044" x .066", will have the specifications set forth in Table III. The coil winding technique shall be essentially similar to the one used for the K500, namely with G-10 spacers at regularly spaced azimuthal intervals. Thickness of G-10 spacers will be 50 mils, width .4", azimuthal spacing of .6".

TABLE III

SPECIFICATIONS OF SUPERCONDUCTOR INSERT

Dimensions:	0.044" x 0.066"
Tolerance:	± 0.001"
Corner Radius:	0.010" ± .001"
Cu/NbTi Ratio:	1.95:1
No. of Filaments:	276
Filament Diameter:	53.7 microns
Min. Thickness of Cu Between Any Two Filaments:	0.00026"
Twist Pitch:	1 inch
Total Length:	200,000 feet
Minimum Length/Piece:	2,000 feet
Critical Current at 5T, 4.2K and 15,000 psi:	Guaranteed: 1200A Expected: 1350A

are listed in Table V.1 and V.2 for the first case, and Table VI.1 and VI.2 for the second. The tables give the field components in kgauss at 1" radial intervals across the coils, as a function of the distance Z from the median plane. The sections α and β of the coils are clearly recognizable on the tables themselves.

The forces acting on the coils were then computed according to these fields and the conductor just discussed. In the first case both coil sections are attracted toward the median plane, the upper one(β) with a total force of 2250 tons, the lower one with just 230 tons. In the second case, i.e. J_α = 3500 A/cm^2 and J_β =-1500 A/cm^2, the upper coil is subject to a force away from the median plane of ≃905 tons while the lower one is still attracted toward the median plane with ≃2130 tons. The contours of constant axial force across the coils, in terms of kilogram per meter of cable length, are shown for both cases in Figs. 9 and 10 respectively.

Radial and hoop stresses have been computed [13] for both limiting cases and the results are shown, in a self explanatory way, in Tables VII and VIII respectively. In these calculations the bobbin is 1" thick, from 44.5" to 45.5" in radius, and the coil structure is fully taken into account, including the G-10 spacers. The banding is assumed to be an aluminum alloy type AC-2219-T87 2" thick. The preload for the cable is of 4190 psi, and for the banding 13540 psi. Only the final data, i.e. after winding, cooling and turning on the magnetic field, are presented in the tables. We refer to (1) for diagrams showing the stresses during the intermediate phases.

There does not seem to be any reason for concern on the

TABLE V.2

UPPER COIL = 3500.00 A/CM2
LOWER COIL = 3500.00 A/CM2

BR TABLE (KGAUSS)

z" ↓ / R" →	45.50	46.50	47.50	48.50	49.50	50.50	51.50
29.000	.286320E 02	.299270E 02	.303640E 02	.300450E 02	.289750E 02	.270810E 02	.248240E 02
26.375	.240340E 02	.258760E 02	.270870E 02	.275740E 02	.274030E 02	.265990E 02	.252110E 02
23.750	.185870E 02	.190640E 02	.192850E 02	.192370E 02	.189200E 02	.183460E 02	.177440E 02
21.125	.130980E 02	.134060E 02	.135900E 02	.137430E 02	.138470E 02	.139160E 02	.141230E 02
18.500	.123900E 02	.144190E 02	.146710E 02	.149310E 02	.151670E 02	.153030E 02	.119960E 02
18.000	.496300E 01	.456800E 01	.522200E 01	.572400E 01	.604800E 01	.612000E 01	.723700E 01
15.400	.694100E 01	.750100E 01	.777600E 01	.786700E 01	.776900E 01	.745700E 01	.739700E 01
12.800	.384200E 01	.420200E 01	.434600E 01	.446100E 01	.453000E 01	.455300E 01	.469500E 01
10.200	.112500E 01	.120200E 01	.126100E 01	.132800E 01	.139100E 01	.142900E 01	.162100E 01
7.600	-.174300E 01	-.188400E 01	-.197400E 01	-.194700E 01	-.179900E 01	-.154400E 01	-.908000E 00
5.000	-.433300E 01	-.393800E 01	-.398900E 01	-.367500E 01	-.300800E 01	-.215100E 01	-.220900E 01
4.000	-.612400E 01	-.729000E 01	-.792200E 01	-.810000E 01	-.776300E 01	-.689000E 01	-.380300E 01
3.000	-.295400E 01	-.101190E 02	-.104830E 02	-.101630E 02	-.908300E 01	-.696100E 01	-.338600E 01
2.000	-.664700E 01	-.810500E 01	-.975800E 01	-.103160E 02	-.101320E 02	-.915500E 01	-.355900E 01

TABLE VI.2

UPPER COIL = -1500.00 A/CM2
LOWER COIL = 3500.00 A/CM2

BR TABLE (KGAUSS)

Z ↓ / R →	45.50	46.50	47.50	48.50	49.50	50.50	51.50
29.000	•726600E 01	•622000E 01	•565200E 01	•546200E 01	•563200E 01	•620100E 01	•671400E 01
26.375	•128420E 02	•119950E 02	•114270E 02	•110880E 02	•109320E 02	•109410E 02	•110620E 02
23.750	•182350E 02	•185330E 02	•186880E 02	•186810E 02	•185380E 02	•183340E 02	•181120E 02
21.125	•237510E 02	•260100E 02	•275260E 02	•282640E 02	•282150E 02	•273930E 02	•256340E 02
18.500	•357640E 02	•380200E 02	•389940E 02	•383620E 02	•361680E 02	•320030E 02	•287240E 02
18.000	•277900E 02	•304670E 02	•349330E 02	•372590E 02	•379050E 02	•368750E 02	•406490E 02
15.400	•247550E 02	•268090E 02	•278070E 02	•278710E 02	•270200E 02	•252740E 02	•227640E 02
12.800	•167790E 02	•178330E 02	•185060E 02	•189240E 02	•190260E 02	•188230E 02	•183500E 02
10.200	•106310E 02	•110890E 02	•113690E 02	•114970E 02	•114640E 02	•112470E 02	•109390E 02
7.600	•485700E 01	•502800E 01	•515300E 01	•534000E 01	•558600E 01	•587900E 01	•641100E 01
5.000	-•530000E-01	•500000E 00	•600000E 00	•104600E 01	•182800E 01	•271600E 01	•335300E 01
4.000	-•226600E 01	-•387300E 01	-•435200E 01	-•440800E 01	-•397600E 01	-•303300E 01	•242000E 00
3.000	-•646300E 01	-•751700E 01	-•780300E 01	-•741500E 01	-•629000E 01	-•409000E 01	-•377000E 00
2.000	-•506300E 01	-•643200E 01	-•801200E 01	-•851600E 01	-•830300E 01	-•732600E 01	-•143400E 01

MSUX-80-275

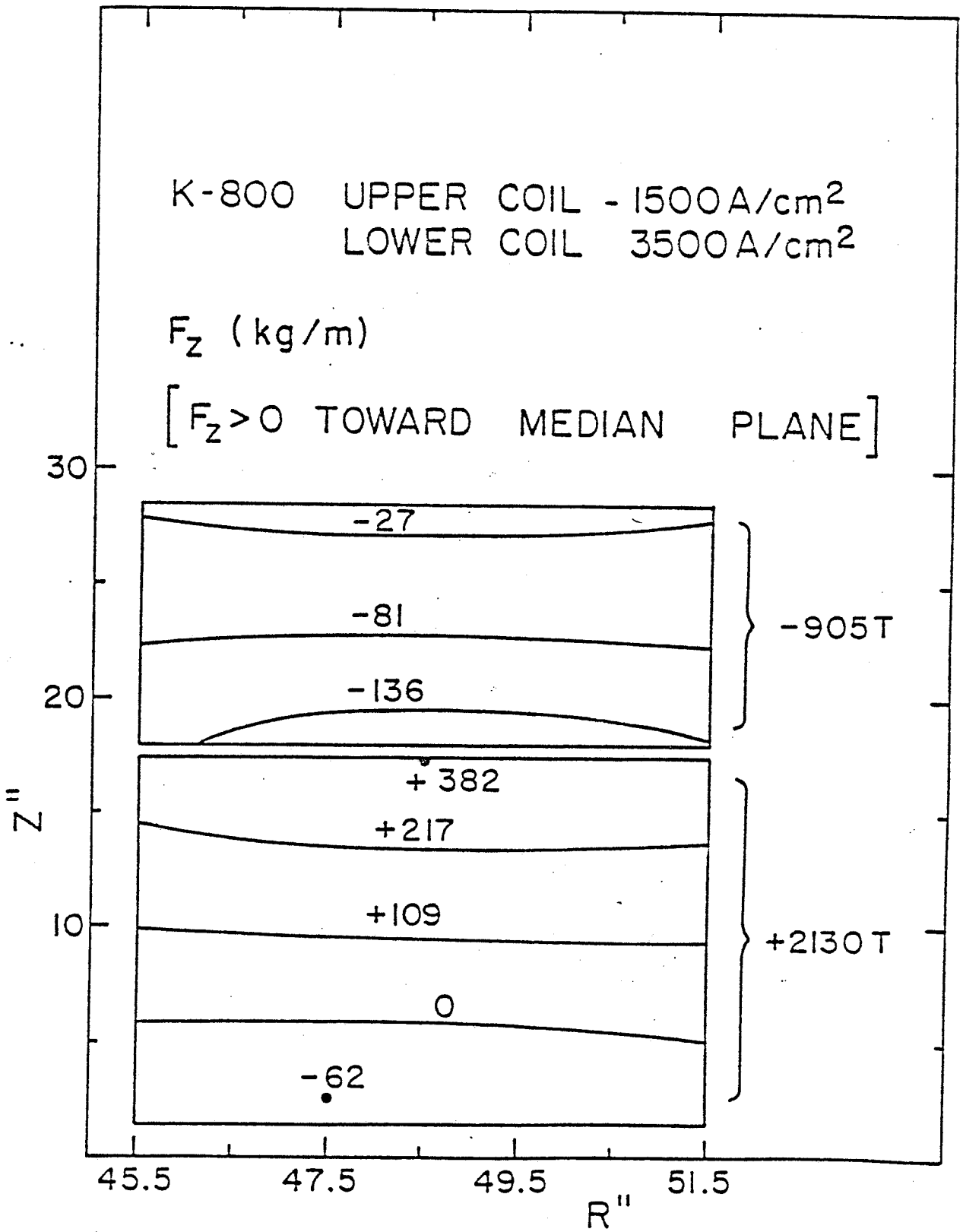

Fig. 10. Contours of constant axial force across the coils, in kg/m of cable length for J_α = 3500 A/cm^2, J_β = -1500 A/cm^2. Total forces on the two coil sections are also indicated.

TABLE VII. RADIAL AND HOOP STRESSES AT J_α = 3500 A/CM^2, J_β = -1500 A/CM^2 †

	RADIAL STRESS (min-max)						HOOP STRESS (min-max)					
Z"	Bobbin		Conductor		Banding		Bobbin		Conductor		Banding	
2	0	-219	-219	-1160	-1036	0	-10492	-10712	6976	2041	27980	26245
4	0	-205	-205	-1210	-1044	0	- 9834	-10039	7318	2462	28169	26441
7.6	0	-223	-223	-1257	-1034	0	-10670	-10892	6833	1923	27901	26163
18	0	-338	-338	-1003	-970	0	-16188	-16526	-1614	3905	26267	24471
18.5	0	-352	-352	-963	-963	0	-16853	-17205	-2040	3571	26079	24277
23.75	0	-428	-428	-922	-921	0	-20480	-20908	-4372	1654	25107	2317
29	0	-440	-440	-915	-914	0	-21066	-21506	-4751	1306	24818	2297

Note: - Negative sign means compression

- Assumes conductor preload of 4.19 kpsi and banding preload of 13.54 kpsi

- All units: psi.

for both hills and valleys, in Fig. 12.

The increase in pole radius, to 42", is quite evident. This choice was prompted by the fact that if the .25" radial gap, necessary for the clearance between the vacuum tank and the pole, is set at 41" as originally devised, the local reduction in the average field and flutter is too high and cannot be properly compensated for. The tank wall thickness was thus reduced to 1", down from the anticipated 2", and consequently the .25" radial gap is between 42" and 42.25". This radius is about 1" farther out than the extraction radius (see Sec. 6) and the effects of the radial gap on the field in this critical edge region are therefore tolerable.

The increase of the minimum hill gap to 3" was dictated by extraction considerations. As reported already in the CDR, and discussed at length in Sec. 4.3 of this report, the operating range of the machine is limited on the low field side by the $\nu_r + 2\nu_z = 3$ resonance. Furthermore, the resonance shows up at progressively smaller radii as the field decreases, an effect also observed in the K500 cyclotron. If the required dynamic range of the cyclotron is to be preserved, it is therefore necessary to move the deflectors progressively inward as the field level is lowered. In the original K800 geometry we are prevented from doing so by the presence on the hill of the trim coils, which have to extend till the radius of 40.5" in order to be effective for the field trimming. As a consequence the axial space available for the electrostatic deflector, which is also positioned in a hill, becomes too restricted. We have therefore increased the hill gap to 3", and at the same time reduced the axial space occupied by the last trim coil by .5". This is accomplished by having just

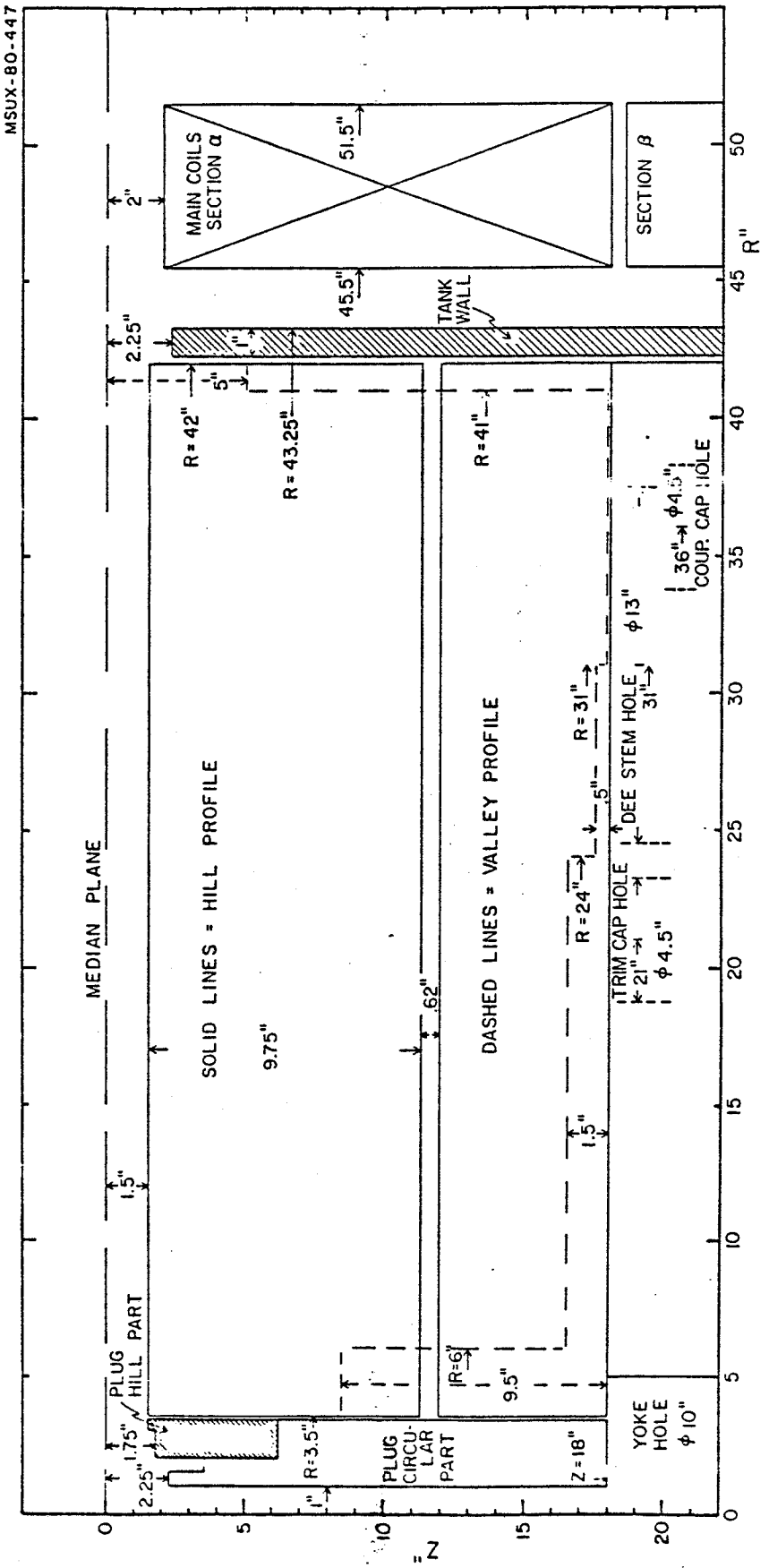

Fig. 12. Hill and valley profiles as a function of radius. Also shown are details of the tank wall and the main coil position.

diameter. This larger hole is desirable for a future axial injection system.[12] The center plug is sketched in Fig. 12 and in greater detail in Fig. 13. The plug design follows closely that of the K500, being composed of a cylindrical part and a hill part. The latter is 33^{o} wide and extends up to 3.37" in radius. A 2" diameter center hole is provided either for the insertion of an ion source, or axially injected beams. The plug extends axially up to 18" from the median plane, compared with the 12" of the K500. All other dimensions are given in a self explanatory way on the figure itself.

Some holes are provided for R.F. purposes, namely:

- a 13" diameter hole for the dee stem, centered at R = 31"
- a 4.5" diameter hill for the trimming capacitor, centered at R = 21"
- a 4.5" diameter hole for the coupling capacitor, centered at R = 36"

In addition there are twenty-two holes along each side of each hill, i.e. 44 holes/sector, of .75" diameter, for the leads of the 22 trim coils anticipated in the machine. These holes are not shown in the figures.

Turning now to a discussion of the sector spiral, Fig. 11, let us first state that the basic spiral constant, i.e. 1/13 rad/inch, has remained substantially unchanged. As mentioned earlier, the transition between the two counter spirals, at R = 15", has been made sharp instead of the smooth one envisaged in the CDR. This way both the pole tips and the trim coils, which will be wound around the latter, are easier to fabricate. As discussed later

the decrease of vertical focusing at the transition radius can be easily compensated for and therefore this solution has been definitely adopted.

As shown in detail in Fig. 14, the hills are 33^{o} wide at R = 3.5",where they begin,and reach a 46^{o} width at R = 15". Henceafter they have a constant width of 46^{o} and follow rigorously a 1/13 rad/inch spiral constant up to a radius of 37.15". There the hill starts widening with a locally increasing spiral angle, as clearly shown by the entrance edge curve of Fig. 14, and reaches a width of 51^{o} at R = 40.2". After it is radial up to R = 42" with a constant width of 51^{o}, a feature already anticipated in the CDR. The rationale for this peculiar geometry is the following:

- in the critical radial range of 37" to 40", the local spiral increase of the order of 2^{o} increases the axial focusing and offsets completely the loss in flutter due to the larger hill gap.

- the hill width increase to 51^{o} compensates for the larger field fall-off determined by the 3" hill gap. Besides, it helps to obtain the right behavior of the average field produced by the iron as a function of radius. The latter, in order to minimize the trim coil power, must flatten out and in fact have a small increase near the extraction radius. This topic will be discussed in more detail in the following section.

- a radial sector in the last 2" in radius decreases locally the ν_z value, where the latter tends to increase sharply due to the average field fall off. Therefore, as explained in the CDR, the radial shape helps in controlling the rapid onset of the $\nu_R + 2\nu_z$ 3 resonance, and pushes outwards

the radius where this happens. The radial cut at R = 40.2" is the optimum on the basis of the presently computed magnetic fields. A different cut, as explained in Sec. 4,may be necessary if measured data show that an improvement of axial focusing is necessary.

For the purpose of easy machining the hill profile has been fitted with arcs of circles. It was found necessary to split the sectors in 5 parts, as indicated clearly in Fig. 11, where the values of the separation radii are also noted.

The coordinates (x,y) of the centers of said arcs of circle, and their radii of curvature are given in Table IX for all different parts. A right handed (x.y) coordinate system with origin in the machine center is assumed, the entrance and exit edges of a sector being labelled α and β respectively. The sector portions are numbered from 1 to 5, 1 referring to the one closer to the center, which begins at R = 3.5" because of the central hole.

TABLE IX. SECTORS MACHINING PARAMETERS +

Section#	R_α	$X_{c\alpha}$	$Y_{c\alpha}$	R_β	$X_{c\beta}$	$Y_{c\beta}$
1	9.872	3.095	9.062	9.748	-3.718	7.951
2	18.630	6.165	-9.680	18.630	11.246	-2.290
3	29.584	-4.604	-11.687	29.584	5.209	-11.430
4	32.825	-5.213	-8.013	35.635	-.789	-10.446
5	radial			radial		

+ All values in inches

$R_{1,2}$ = 15" $R_{2,3}$ = 25.3" $R_{3,4,}$ = 37.15" $R_{4,5}$ = 40.2"

TABLE X. TRIM COIL RADII

Trim Coil #	R_i (inches)	R_{fm} (inches)	Notes
1	3.75	4.95	one turn less on
2	5.05	6.25	each layer
3	6.65	8.10	
4	8.20	9.65	
5	10.05	11.50	
6	11.60	13.05	
7	13.45	14.90	→ 15" transition
8	15.10	16.55	radius
9	16.95	18.40	
10	18.50	19.95	
11	20.35	21.80	
12	21.90	23.35	
13	23.75	25.20	→ 25.3" pole tip
14	25.40	26.85	splitting
15	27.25	28.70	
16	28.80	30.25	
17	30.65	32.10	
18	32.20	33.65	
19	34.05	35.50	
20	35.60	37.05	→ 37.15" pole tip
21	37.65	39.10	splitting
22	39.20	40.65	→ Last trim coil has one layer only, of 5 turns

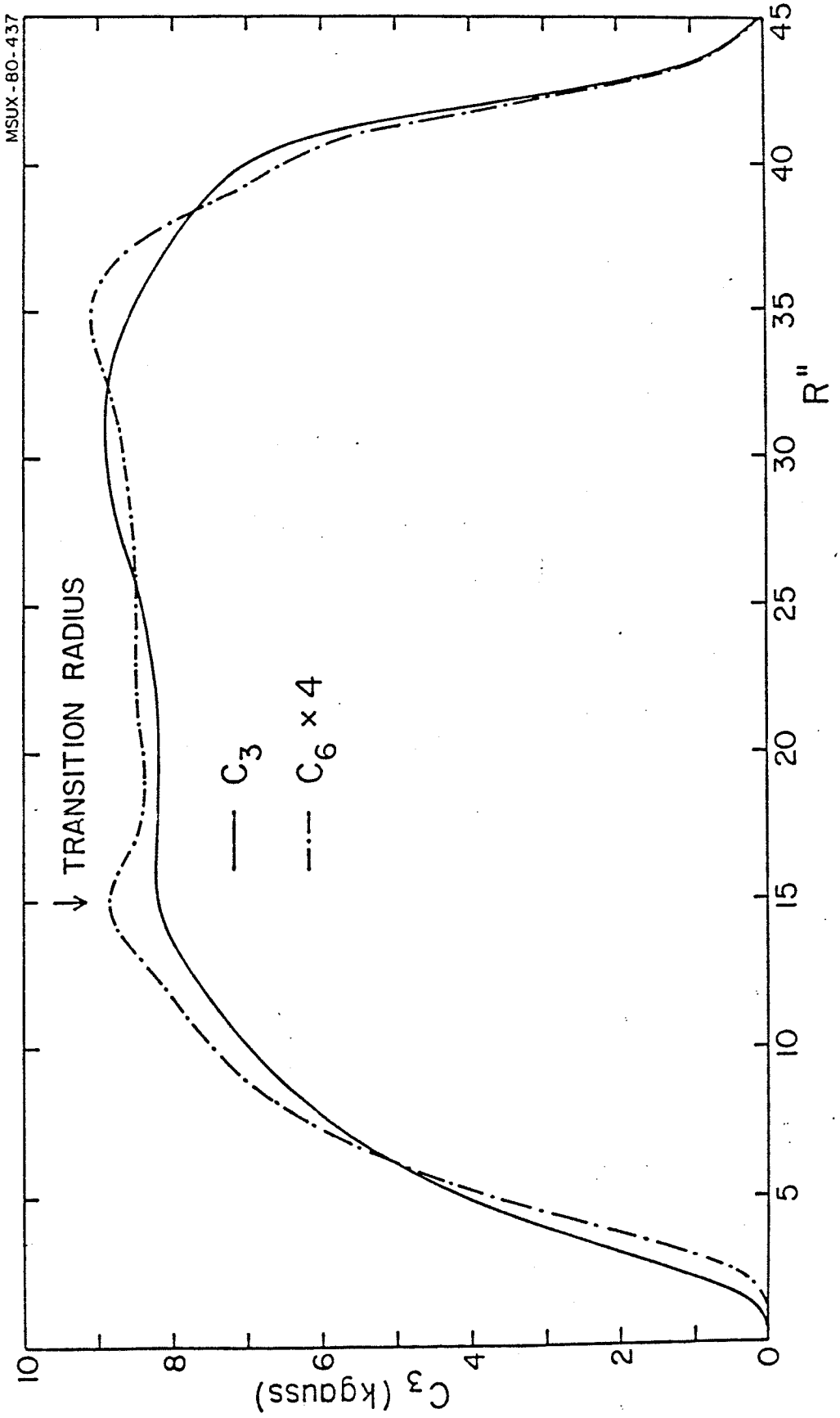

Fig. 15. Amplitude of the third and sixth field harmonics, as a function of radius, calculated according to the saturation hypothesis.

were carried out at the following J_β values,again in A/cm^2: -2000, -1000, 0, 1000, 2000, 3000, 4000. As a glance at Fig. 8 shows, this grid covers completely the dynamic range of the machine.

At an excitation of J_α = 3250 A/cm^2 and J_β = -1000 A/cm^2, which is close to the one needed for acceleration of 200 MeV/n fully stripped light ions, the average field produced by the iron is as shown by the solid line in Fig. 17. Also shown for comparison is the theoretical best field needed, according to the principles set forth in ref (5) to minimize the overall trim coil power. The difference, apart from the central region up to a few inches in radius where the plug produces a field cone, is confined to $\pm$ 20 - 30 gauss at most, i.e. well within the TRIM code accuracy.

The present configuration is therefore very satisfactory. It may be worthwhile to discuss the difference between the iron field obtained with a 3" and a 2.5" hill gap. This is shown in Fig. 18. The main change is just a slight change in the field level. Also, as expected, the field fall off is somewhat more accentuated with the larger hill gap. None of these differences, however, play any significant role on the field properties and henceforth on the machine performance.

After magnetic field data are available, it may be necessary to shim the hill locally at radii between 38" and 41" in order to correct for the 25-30 gauss differences which are presently observed between the calculated field and the theoretical "best" field. Calculations show that this can be accomplished with a shim,at most 40 to 60 mils thick, in this particular region.

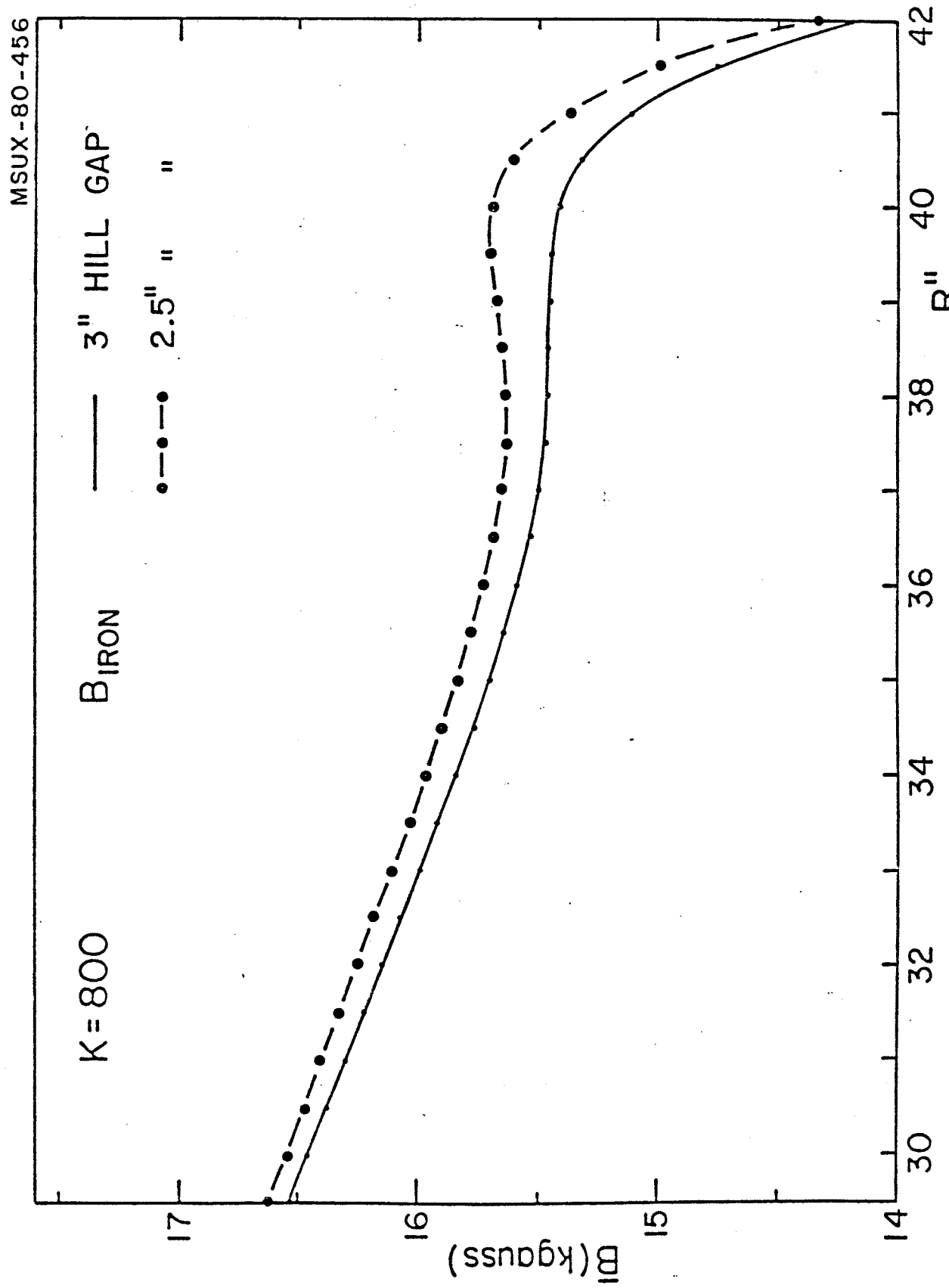

Fig. 18. Iron produced field, at outer radii only, with a 3" and a 2.5" minimum hill gap.

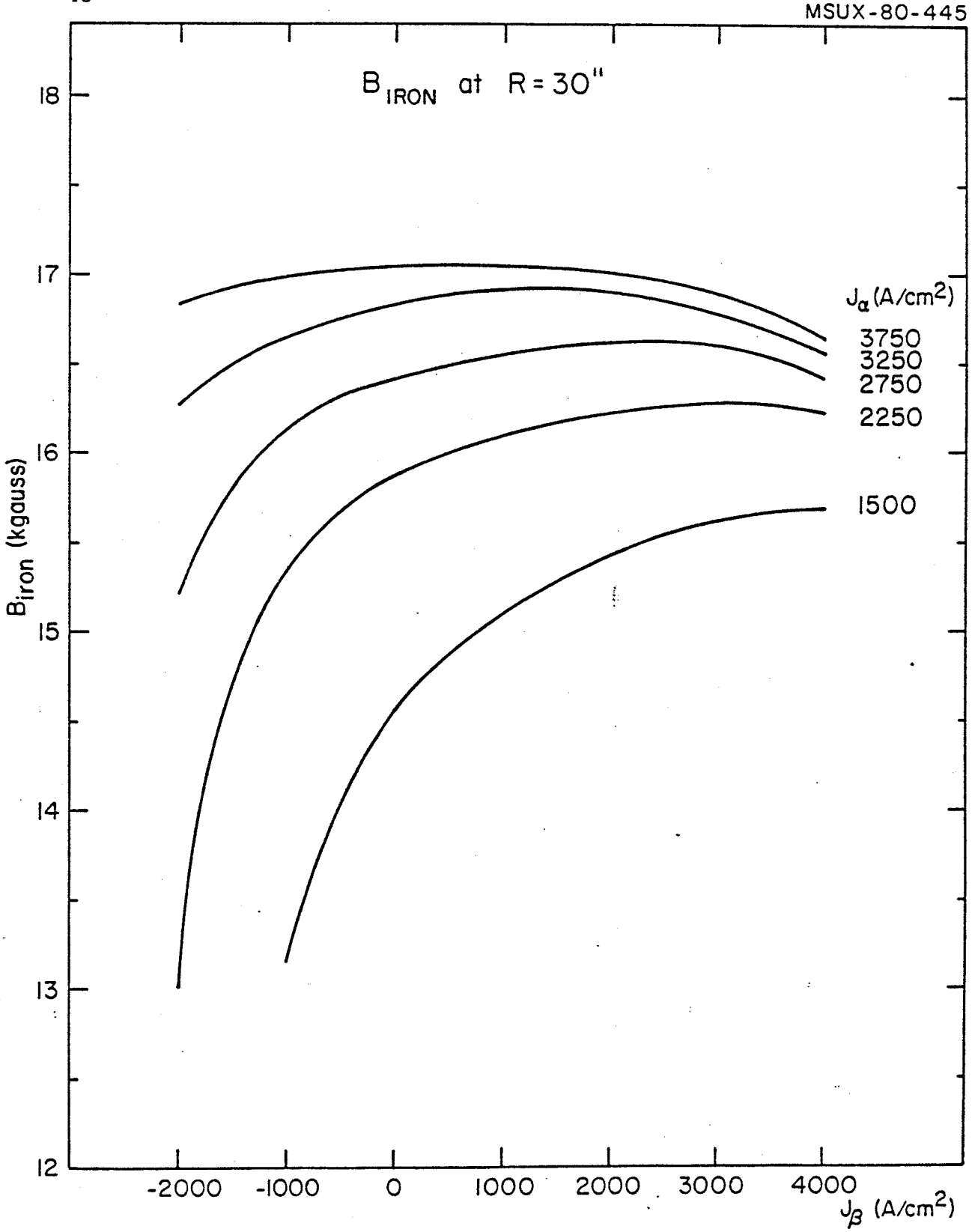

Fig. 19. Variations of the iron produced average field, at a radius of 30", over the J_α, J_β grid used for TRIM calculations (see text for details).

A summary of the results for the twelve ions chosen along the boundary of the operating diagram is given in Fig. 21. Both current densities J_α and J_β, the trim coil power and the relevant energy/nucleon are given for each ion. As seen from the figure, the upper limiting case in terms of J_α and J_β is about 3100 A/cm^2 while the lower one is J_α = 3500 A/cm^2, J_β = -1500 A/cm^2 and corresponds to the most relativistic ions at 200 MeV/n. The trim coil powers correspond to a field fitting which includes the proper shaping of the field in the transition region at R = 15", as described in Sec. 4.2. Contours of constant trim coil powers, across the operating diagram, are shown in Fig. 22. The values given in the latter figure do not include, however, the requirement for the transition region, but a comparison between the two shows that the difference is rather small. In any case, currents are below a maximum operating limit of 400 A for any trim coil.

As for the trim coil efficiency, the increase in the hill gap from 2.5" to 3", which entails a larger distance of the coils from the median plane, has not generated a sizable increase in the necessary trim coil currents. The reason, as shown in Fig. 23, is that while the value of the peak field has decreased, the slope becomes less steep. The latter effect tends to compensate for the former.

Examples of the trim coil currents needed to isochronize the field for different ions are shown in Fig. 24. The ions, as a glance to Fig. 21 confirms, have been chosen so as to represent limiting cases over the operating diagram. Note that the current pattern practically reverses in going from the ion with Z/A = .5,

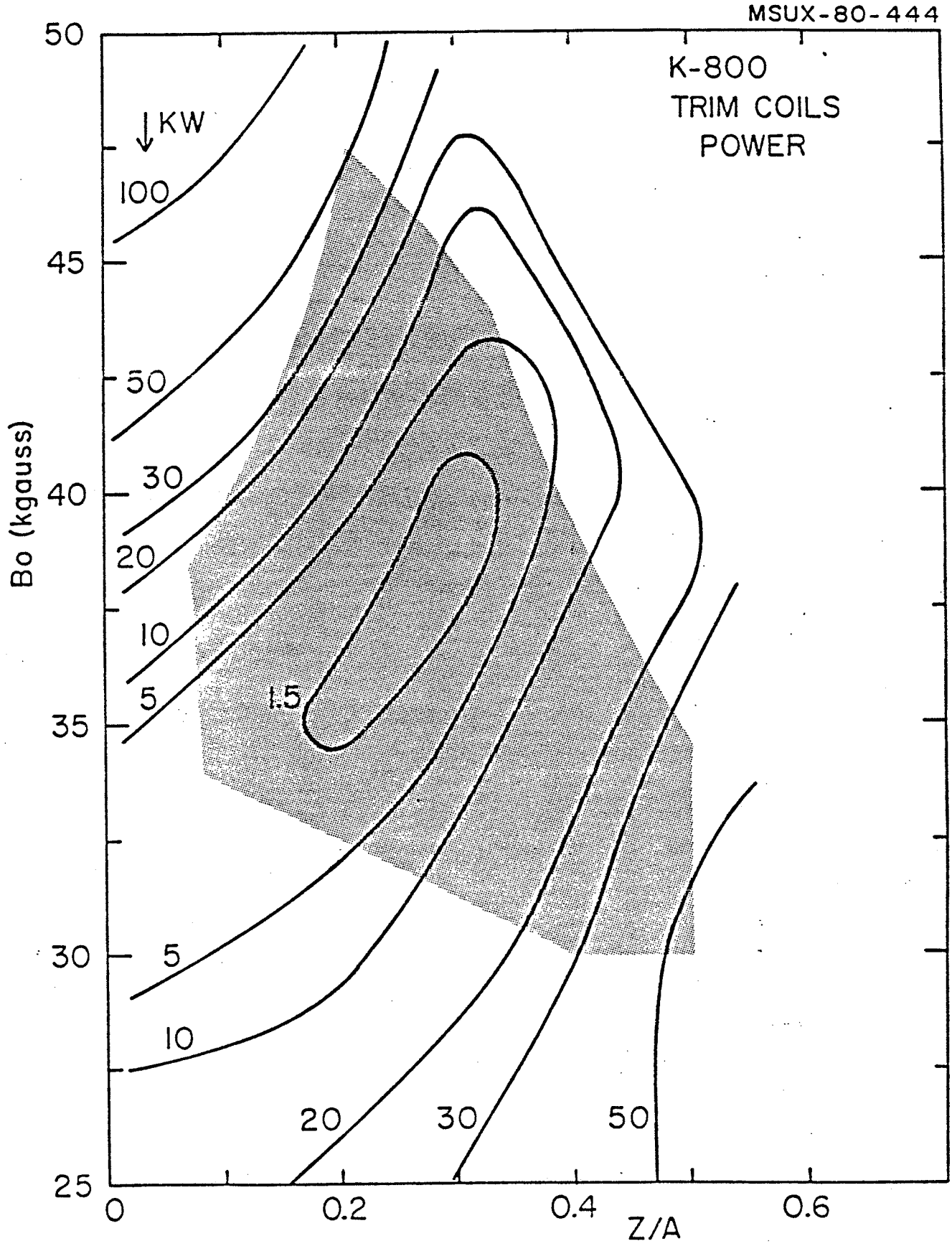

Fig. 22. Constant trim coil power lines, labelled by their kW values, across the (B_o, Z/A) operating diagram.

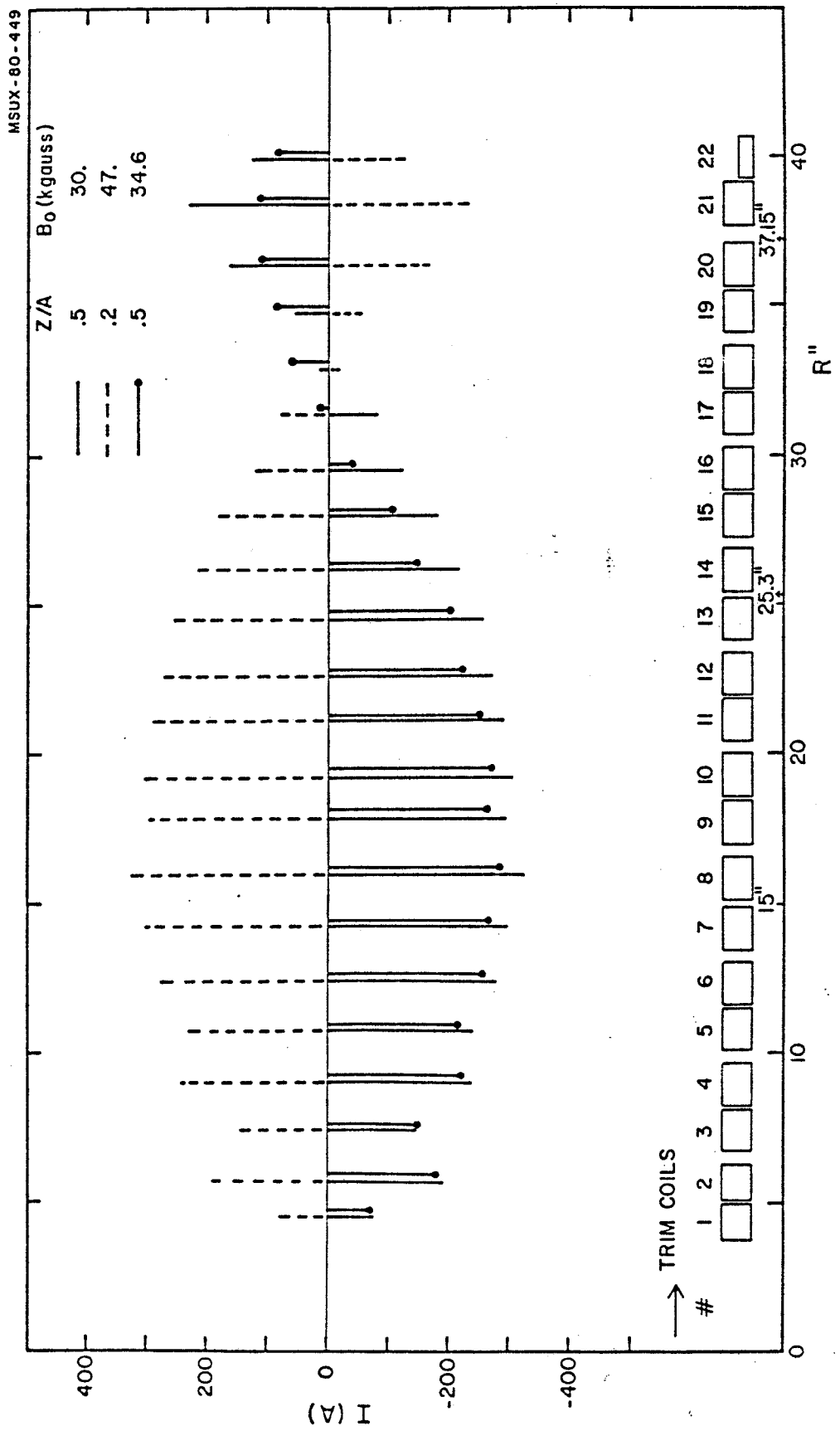

Fig. 24. Trim coil currents for various ions. The trim coil geometry is sketched at the bottom, as a function of radius.

B_o = 30 kgauss to one with Z/A = .2, B_o = 48 kgauss. The trim coil geometry is sketched at the bottom, and as discussed earlier, the last trim coil has only one layer of 5 turns. Its current is still, though, much less than the 400 A limit. The corresponding total field contributions from the trim coils for the same ions are shown as a function of radius in Fig. 25. The maximum field is about 300 gauss, at the machine center. A positive sign means that the trim coil field adds to the main field and vice versa.

The resulting total average fields, axial focusing frequencies and accelerating phase are shown in Fig. 26 for fully stripped light ions, Z/A = .5, and two different center field levels. The two levels of 34.6 and 30 kgauss correspond to the maximum and minimum values for these ions (see Fig. 21) and to a final energy of 200 and 137 MeV/n respectively. Likewise, similar plots are presented in Fig. 27 for ions with Z/A = .32, corresponding in the (B_o, Z/A) plane to the intersection of the bending and focusing limit, and in Fig. 28 for Z/A = .2. The latter charge state, at the maximum field level of 47 kgauss, represents the most rigid beams available. For every ion, two cases with maximum and minimum center field values are presented, other details being given on the figures themselves.

A few comments are in order:

- as shown by the phase curves, the total fields thus obtained have excellent isochronous properties

- in correspondence of the transition region between the two spirals at R = 15", and also just before the extraction, we accelerate above the isochronism in order to enhance the axial

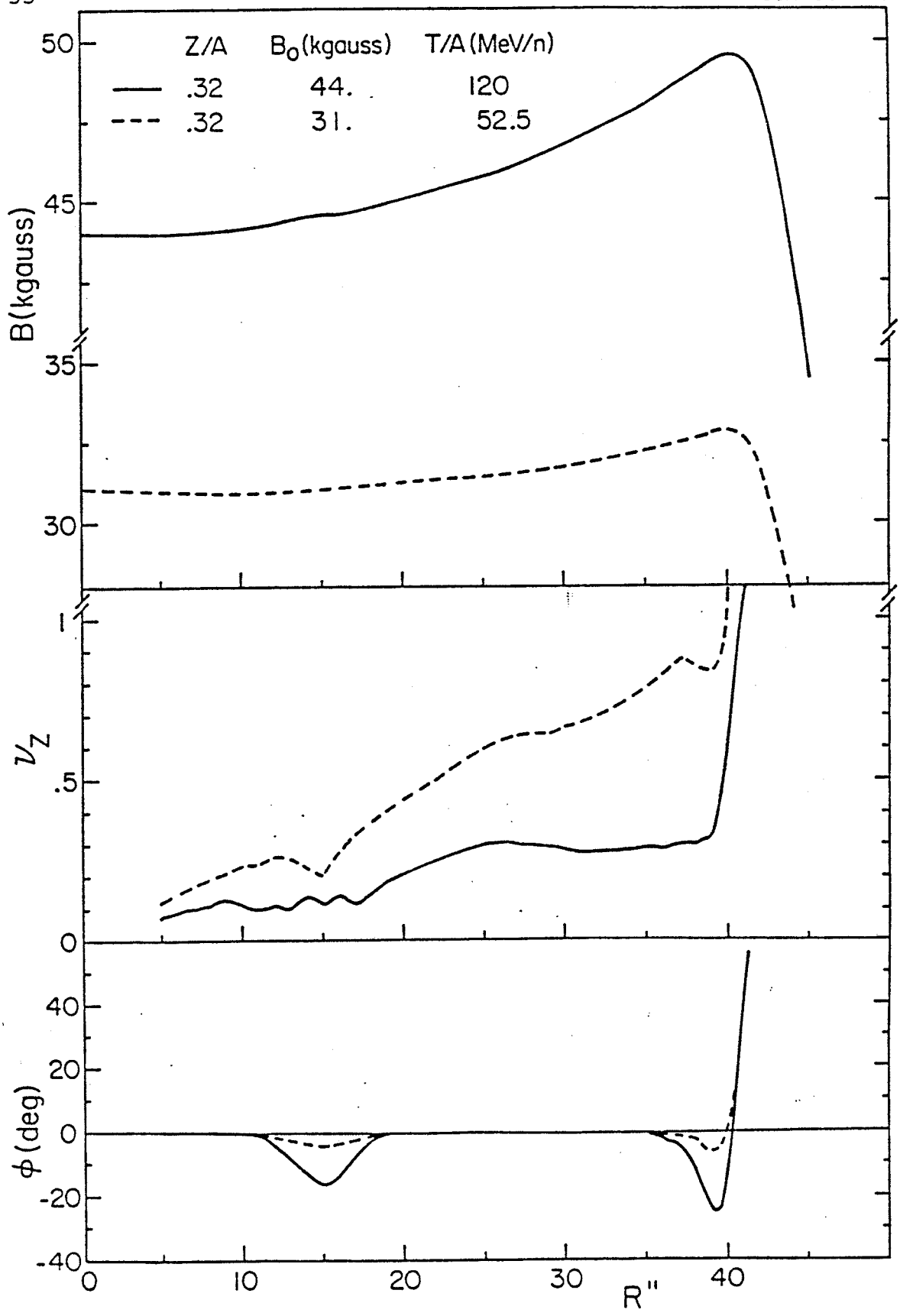

Fig. 27. Average total field, focusing frequency, and accelerating phase for Z/A = .32 ions and two different center field levels.

focusing there. The transition region is discussed in more detail in the following section. As for the extraction region, the maximum negative phase shift thus introduced, Fig. 26, is about 25°, the corresponding minimum ν_z value being about .2. For the most relativistic ions, extraction occurs typically at a positive phase not exceeding $\approx 30^{\circ}$.

- oscillations in the ν_z curves, less visible in the phase curves, are induced by the trim coil contributed fields. This effect is explained in detail in ref. (7), in connection with the K500 cyclotron.

- should a larger axial focusing be needed near extraction, an issue which may arise after magnetic field data are available, the most likely parameter to be used is the extent of the radial cut in the hills, as shown in Fig. 29. If the radial cut of the sector spiral starts at R = 40.8" instead of starting at R = 40.2" as in the present configuration, a sizable increase in ν_z near the extraction radius is produced. As a consequence, the $\nu_R + 2\nu_z = 3$ resonance moves somewhat towards smaller radii, but the amount of movement is quite small, as shown in the lower half of Fig. 29, and therefore does not jeopardize the extraction. This possibility should then be kept in mind if, for example, the measured flutter turns out to be smaller than calculated, a fact indeed observed in the K500 cyclotron.[6]

4.2 The transition region at R = 15"

The loss of axial focusing in the transition region at R = 15", where the sectors go radial, is particularly sensitive for very relativistic ions. For example in the case of 200 MeV/n the axial

frequency ν_z would be imaginary if the ions were accelerated in a perfectly isochronous field. The average field gradient must then be changed locally as shown in Fig. 30, where the solid line represents the actually fitted field while the dashed line is the theoretical isochronous field. Fitting to this adjusted field produces the axial focusing frequency shown on top of Fig. 30, i.e. a very acceptable one. The corresponding phase shift, derived from accelerating above isochronism before R = 15", and below isochronism thereafter, was already shown for all ions in Figs. 26 to 28.

As apparent from Fig. 30, the field adjustment needed for compensating the loss in axial focusing encompasses a radial range of approximately $\pm$ 3" around the transition radius.

There are three ways one can accomplish this field correction, namely:

- local shimming of the iron
- using the trim coils
- a combination of these two

We have selected the third option as the most flexible. In fact doing it using only the trim coils would put an unnecessary strain on their currents while doing it with only iron shims makes the adjustment practically the same at all field levels and for all particles, which is not desirable. In this respect, let us recall that since the flutter is proportional to the inverse square of the average field, the compensation needed is much less marked at low than at high fields.

The shimming we have designed is shown in Fig. 31. A 40 mil thick, 1" wide shim is positioned between R = 13" and R = 14", on top of the hill. A 40 mil cut, also 1" wide, was tested on the hill top between R = 16" and R = 17". The resulting field correction is shown by the curve of Fig. 31, and goes obviously in the sense of producing the desired field gradient inversion. The trim coils are then used to add an extra amount of field correction if required. For the extreme case of the 200 MeV/n beam, this is shown in Fig. 32. The dashed line represents the field contribution from the trim coils for a fit to an isochronous field, i.e., the field also shown by a dashed line in Fig. 30. The solid line refers instead to a fit to the adjusted field, i.e., it represents the trim coil contribution when the total field is the one shown by a solid line in Fig. 30. The corresponding variation in the trim coil current pattern is shown in the lower half of Fig. 32. The variations are quite contained, and in no case does the maximum current exceed 400 A. Without the shimming this could instead happen.

In any case, since the precise field behaviour around the transition region will not be known, at the 20-30 gauss precision level, until measured data are available, a decision regarding the shimming and its geometry will have to wait until then. The present results imply, however, that no particular problems should arise in properly adjusting the field in the transition region, even if options different from the ones discussed here are selected.

4.3 The extraction region and the $\nu_R + 2\nu_z = 3$ resonance

The equilibrium orbit properties near extraction have been studied in detail in order to single out the most important aspects

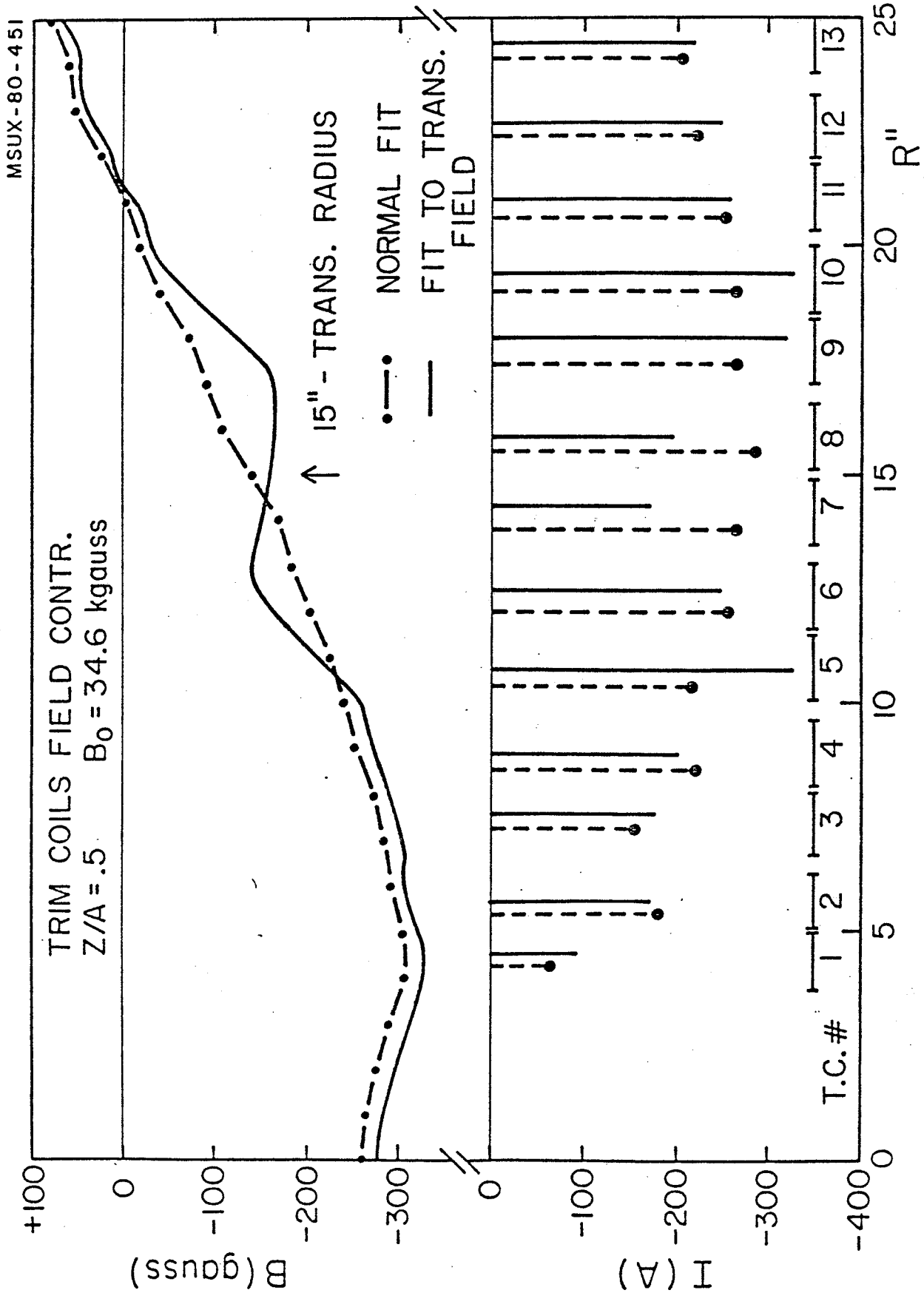

Fig. 32. Field correction produced by the trim coils for a fit to a normal isochronous field (dashed line) and a fit to the adjusted field in the transition region (solid line). The variations of the trim coils currents are shown in the lower half of the figure.

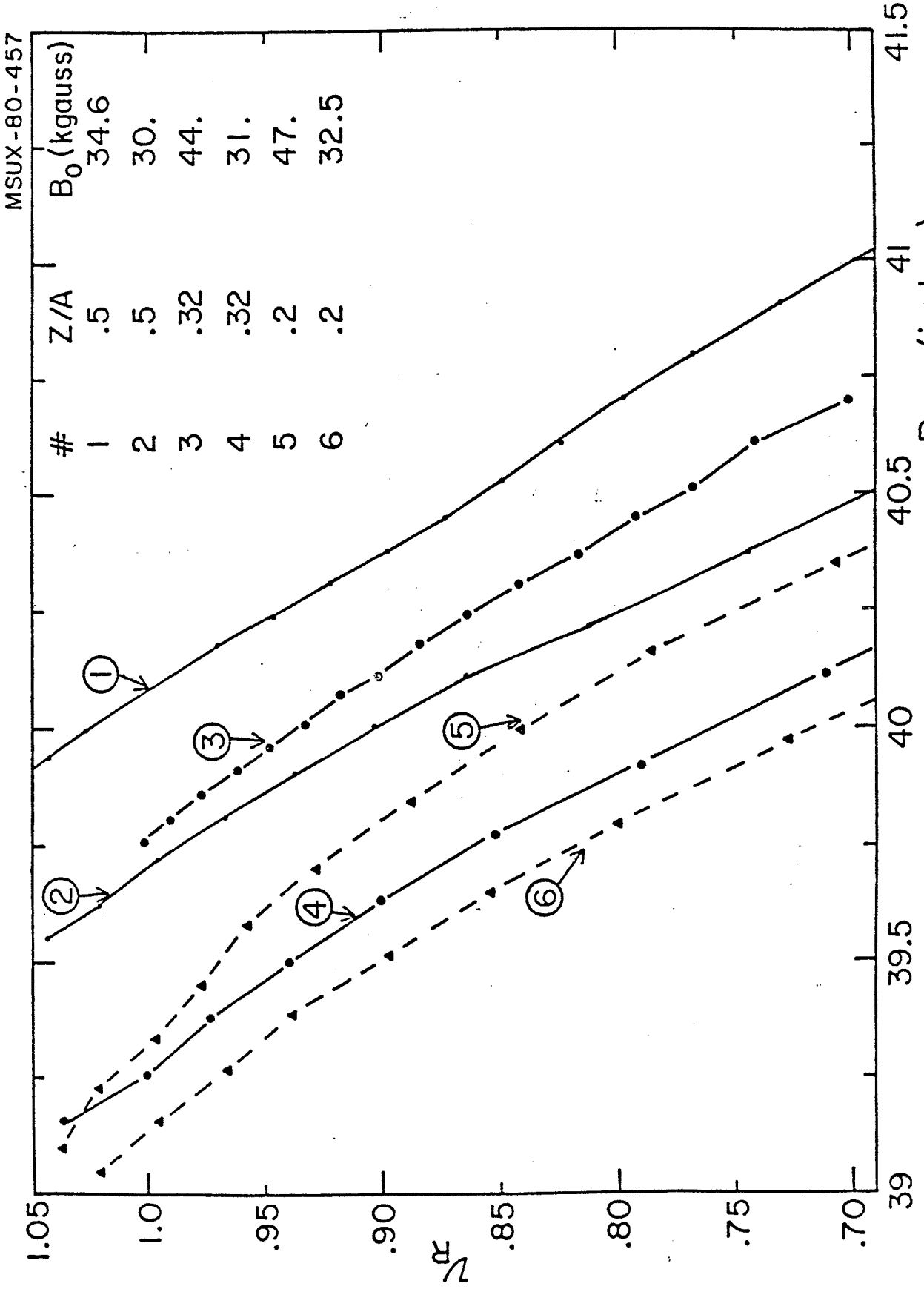

Fig. 33. Radial focusing frequency, ν_R as a function of the equilibrium orbit radius for different charge states and center field values.

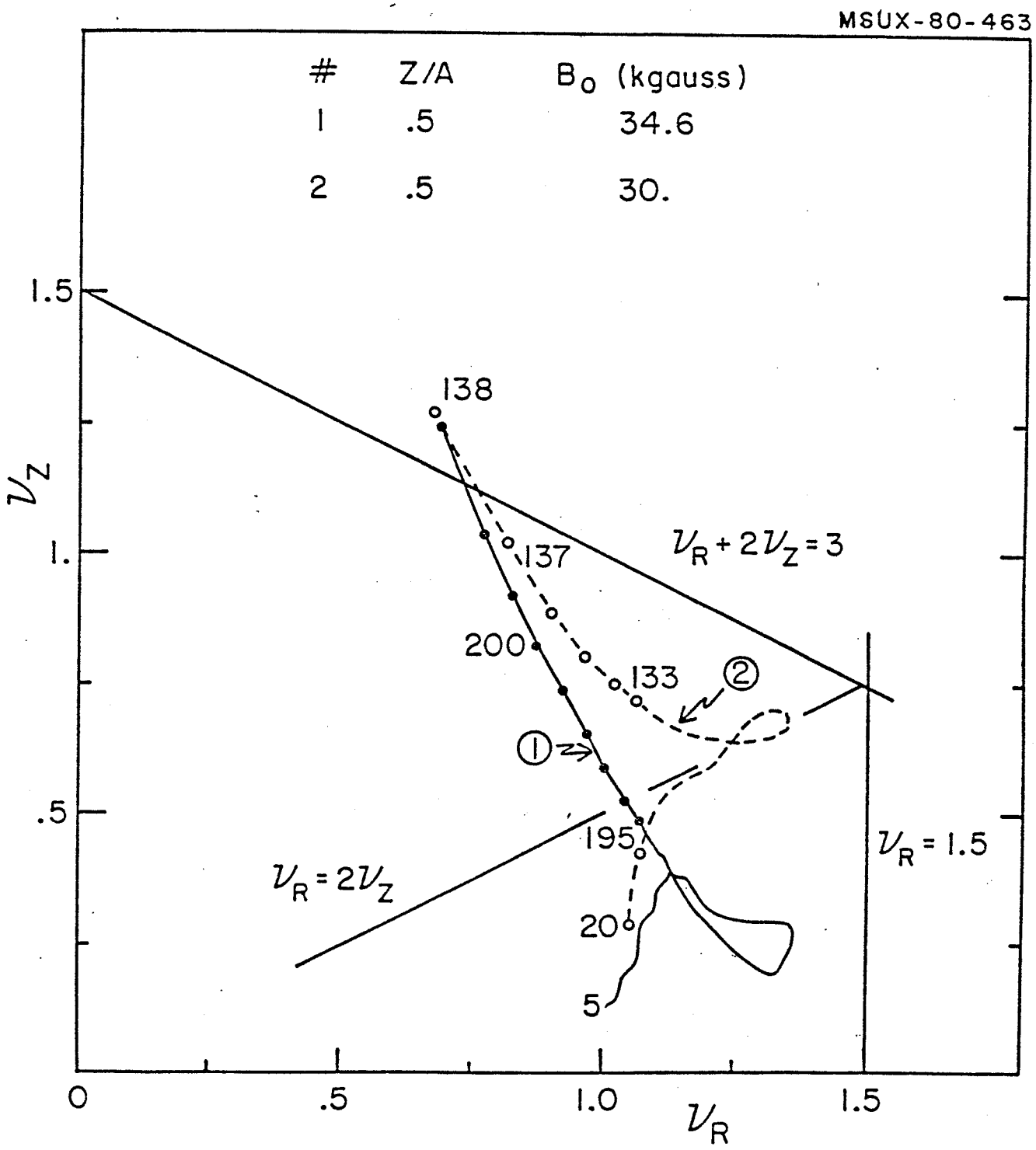

Fig. 34. Working path in the (ν_R, ν_Z) plane and a Z/A = .5 ion at both maximum and minimum center field values. Numbers on the curves refer to energies in MeV/n.

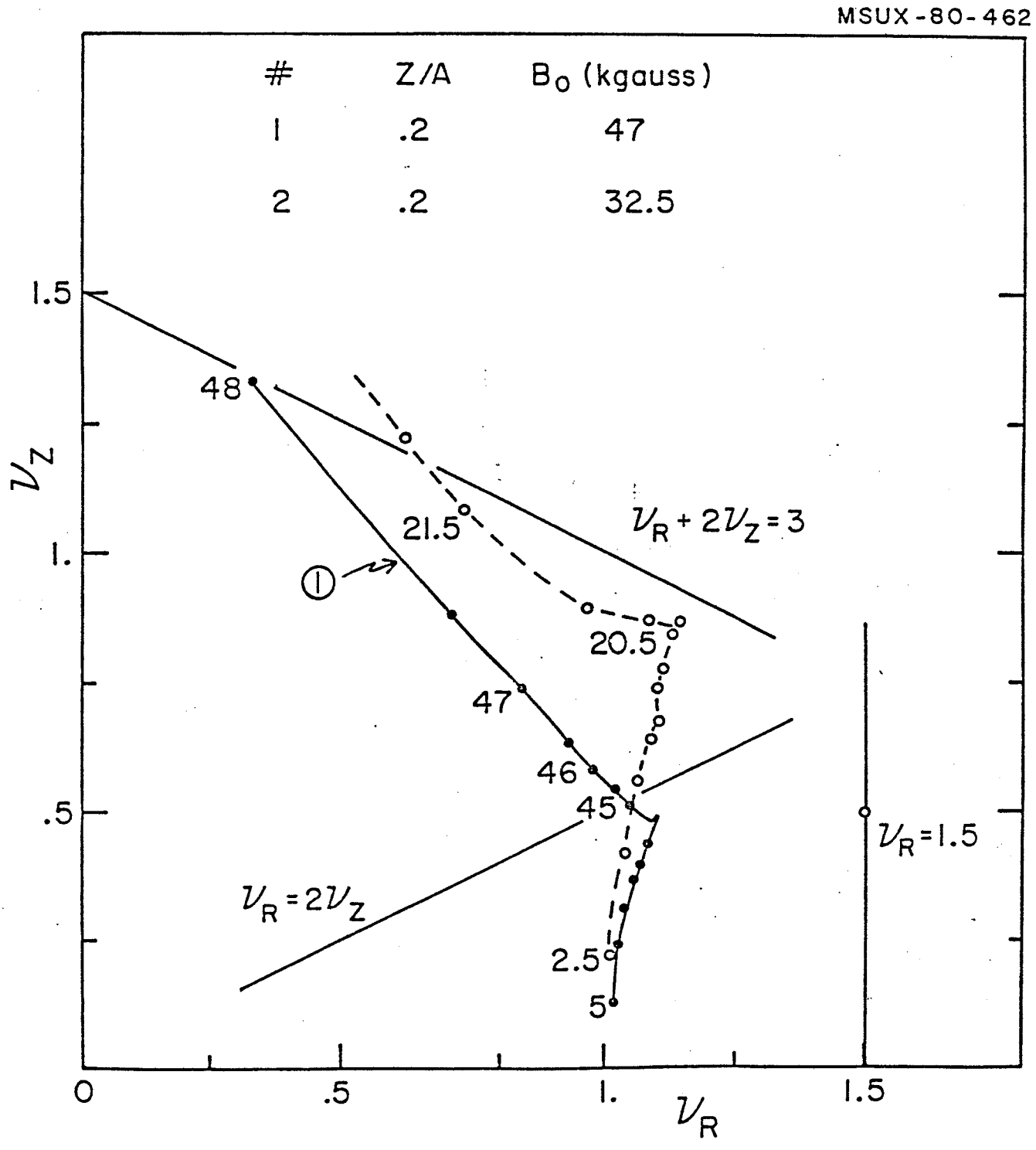

Fig. 36. Working path in the (ν_R, ν_Z) plane for a Z/A = .2 ion at both maximum and minimum center field values. Numbers on the curves refer to energies in MeV/n.

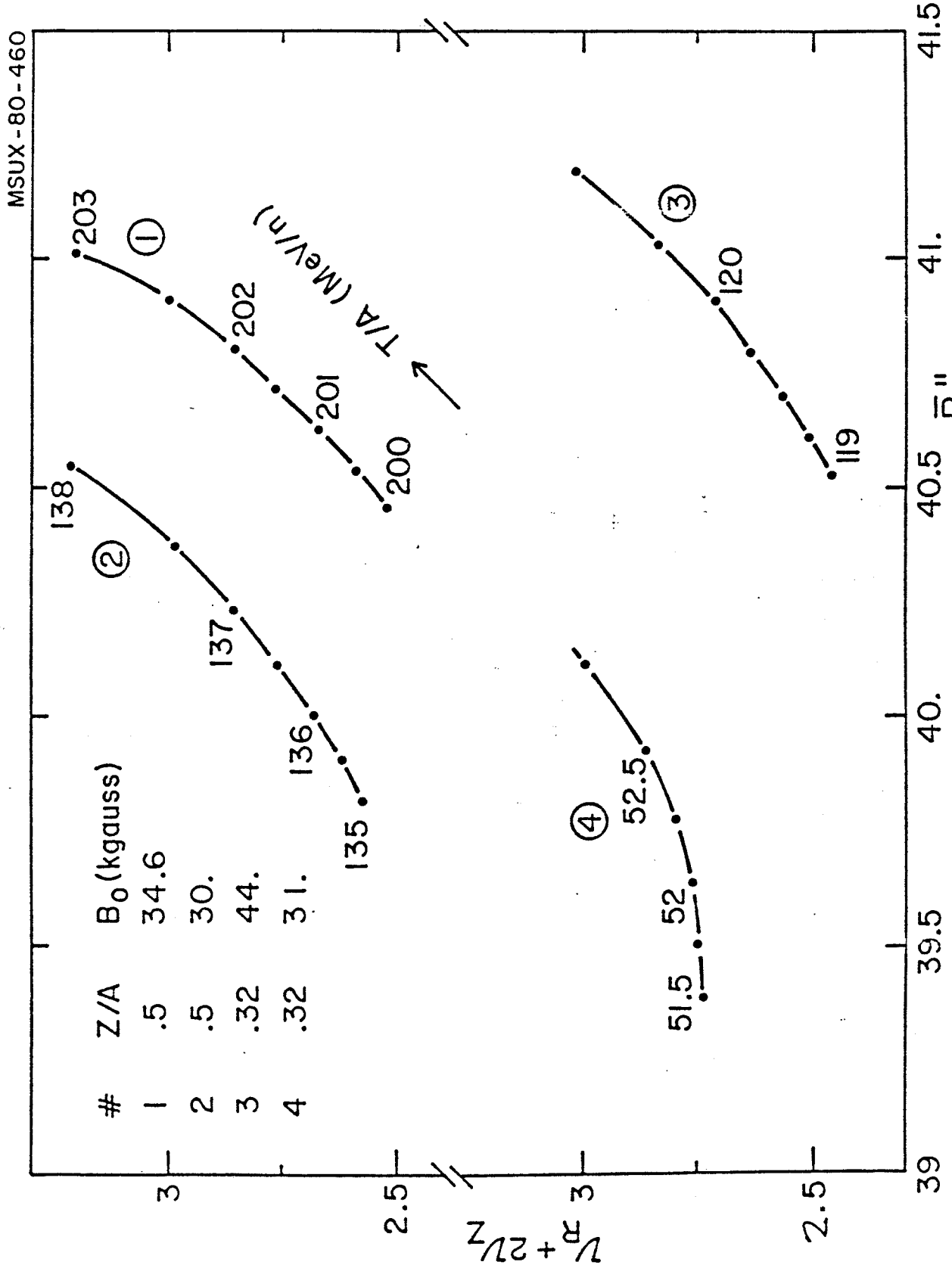

Fig. 38. $\nu_R + 2\nu_Z$ values near extraction for Z/A = .5 and Z/A = .32 ions, as a function of radius. Cases with both minimum and maximum center field values are presented for each ion.

in Sec. 2, it is this requirement that prompted us to increase the hill gap to 3" and reduce the last trim coil to one layer only. In this way the electrostatic deflector can be moved inwards and slide over the last trim coil when needed. More details on these construction aspects are given in the next section.

5. Extraction

The extraction scheme of the K800, as now envisaged, is presented in Fig. 40. As opposed to the CDR, the scheme involves two electrostatic deflectors instead of three. Nine magnetic channels of the passive type used in the K500 are provided along the extraction path. The first and second harmonic components of the field perturbation produced by these channels have to be compensated. For this purpose three compensating bars, labelled by C's in Fig. 40, are anticipated. Needless to say all elements must be radially movable, to within $\pm$ .35" at least.

A list of the azimuthal position of each element, the maximum electric field in the deflectors, and the values of the bias field and magnetic field gradients in the channels are given in Table XI. Also listed are the minimum and maximum radial values of the center ray in correspondence to each element. The latter should be intended, at this stage, as indicative only. In fact, they refer to just two cases, namely an ion with Z/A = .5 at the maximum and minimum field. When the study is completed for all ions, the radial range of positions will certainly be larger, in the sense indicated by Fig. 39.

The present scheme looks satisfactory so far. The reduction from three to two electrostatic deflectors simplifies

the construction problems, and the maximum elctric field of 140 kV/cm is still very much a realistic figure.

As apparent from Table XI, three different channels are anticipated, characterized by gradients of 5.8, 7.5 and 9 kgauss/inch respectively. These variations are accomplished by varying the relative geometry and dimensions of the iron bars constituting the channels. An example of the channel needed for a 7.5 kgauss/inch gradient is shown in Fig. 41. Both the channels and the electrostatic deflectors are very much similar in engineering design to those used for the K500 cyclotron, ref. (9), where more details can be found. In particular, the deflectors are supported by insulators and radially driven by push rods. Cross sections of the first deflector E_1 at the location of an insulator and a driving mechanism are shown in Fig. 42 and 43 respectively.

The main difference with respect to the K500 is that, as anticipated earlier, the deflector can move over the last trim coil thus extracting the beams at the innermost radii before the $\nu_R + 2\nu_Z = 3$ resonance is hit. This is clearly seen in both Figs. 42 and 43. No such need exists for most magnetic channels, because, with the exception of M_1, they are at farther out radii.

So far, phase space diagrams of the accelerated beams prior to extraction look encouraging, although no data are yet available for a fully consistent magnetic field, i.e. one which includes the field perturbations generated by the magnetic channels and their compensation. An example of the beam to beam separation obtained for Z/A = .5 ions at both maximum and minimum fields is shown in Figs. 44 and 45 respectively. Note that in both cases the resonant beam precession at the crossing

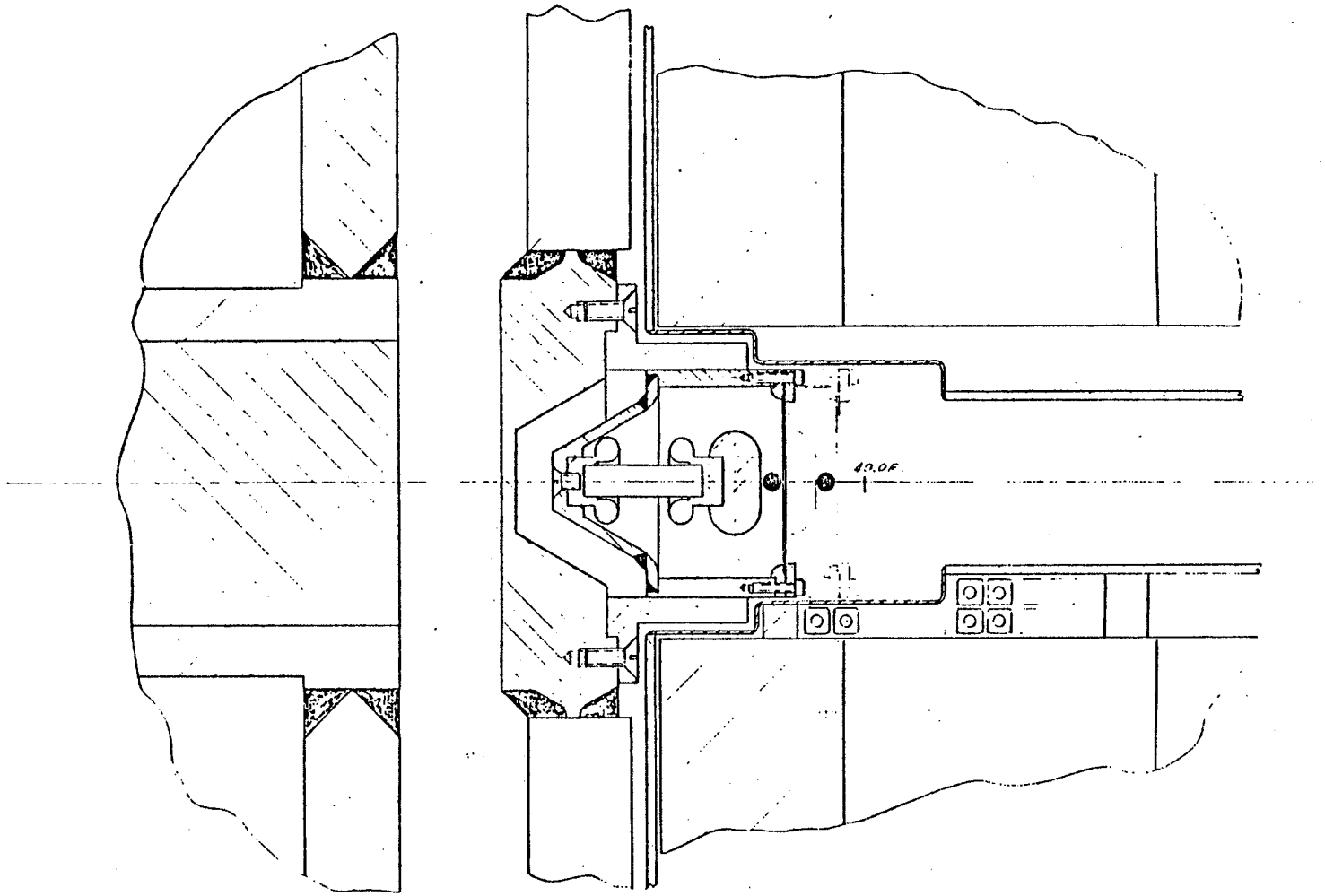

33 1/2°

Fig. 42. Cross section of an electrostatic deflector at the position of an insulator ($\theta = 33.5^{\circ}$).

TABLE XI. EXTRACTION ELEMENTS PARAMETERS

ELEMENT	θ_m (deg)	θ_{fm} (deg)	E_{MAX} (kv/cm)	ΔB (kgauss)	$\partial B/\partial x$ (kgauss/inch)	CENTER RAY RADII (inches) min/max at θ_m	CENTER RAY RADII (inches) min/max at θ_{fm}
E_1	32	92	140	-	-	40.25	40.65
						40.82	41.20
M_1	150	160	-	-2	5.8	40.9	41.43
						41.5	41.86
E_2	162	198	140	-	-	41.53	42.27
						41.93	42.52
M_2	200	212	-	-2	5.8	42.27	42.17
						42.52	42.52
M_3	260	266	-	-2	7.5	42.65	42.82
						43.08	43.22
M_4	270	276	-	-2	7.5	42.95	43.18
						43.34	43.53
M_5	293	299	-	-2	7.5	43.92	44.21
						44.20	44.48
M_6	310	316	-	-2	5.8	44.80	45.10
						45.05	45.35
M_7	318	324	-	-2	5.8	45.58	46.0
						45.81	46.22
M_8	326	332	-	-2	9	46.2	46.75
						46.45	46.92
M_9	340	346	-	-2	9	48.31	49.68
						48.44	49.80

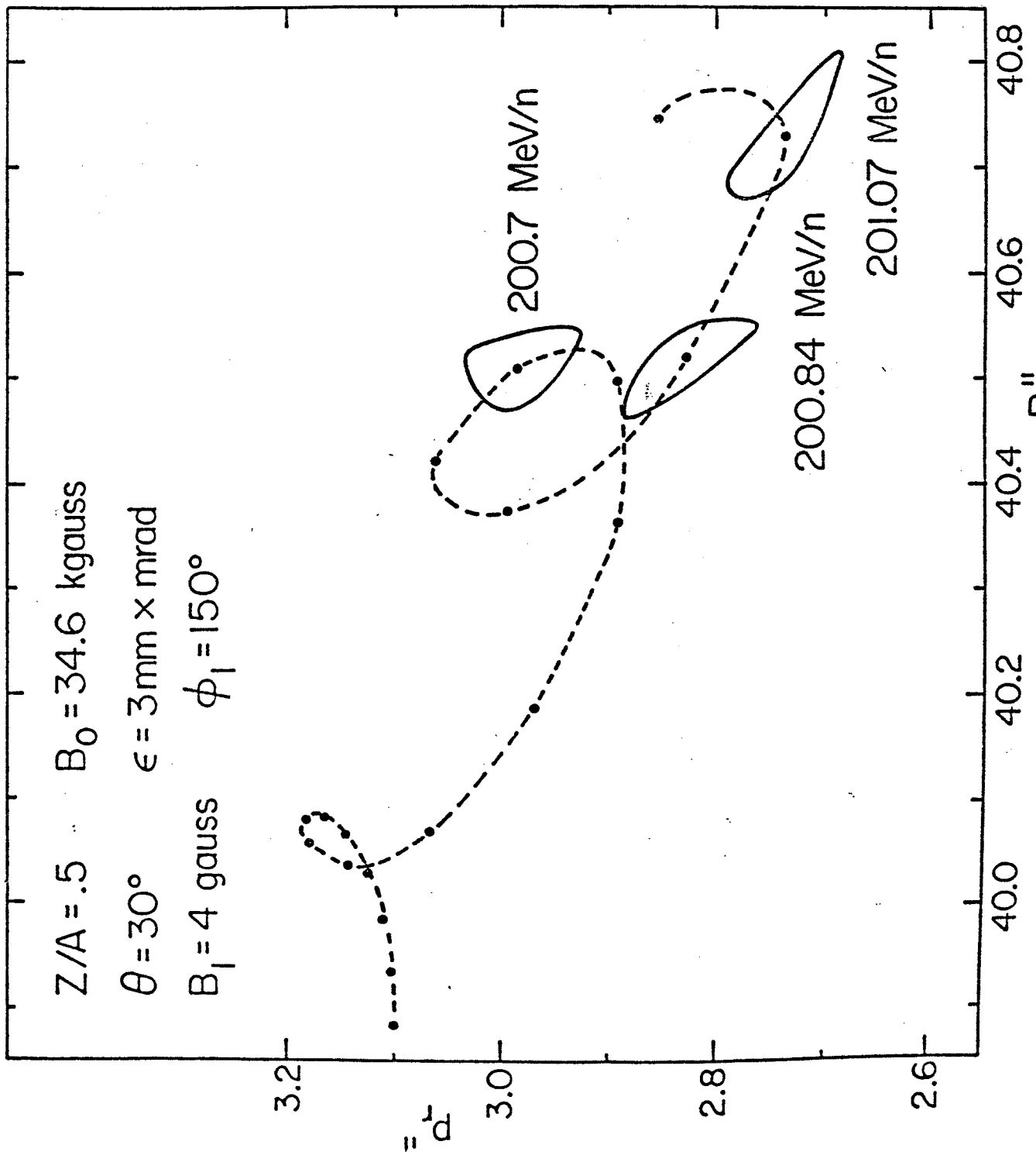

Fig. 44. Radial phase space of ≈200 MeV/n beam prior to extraction.

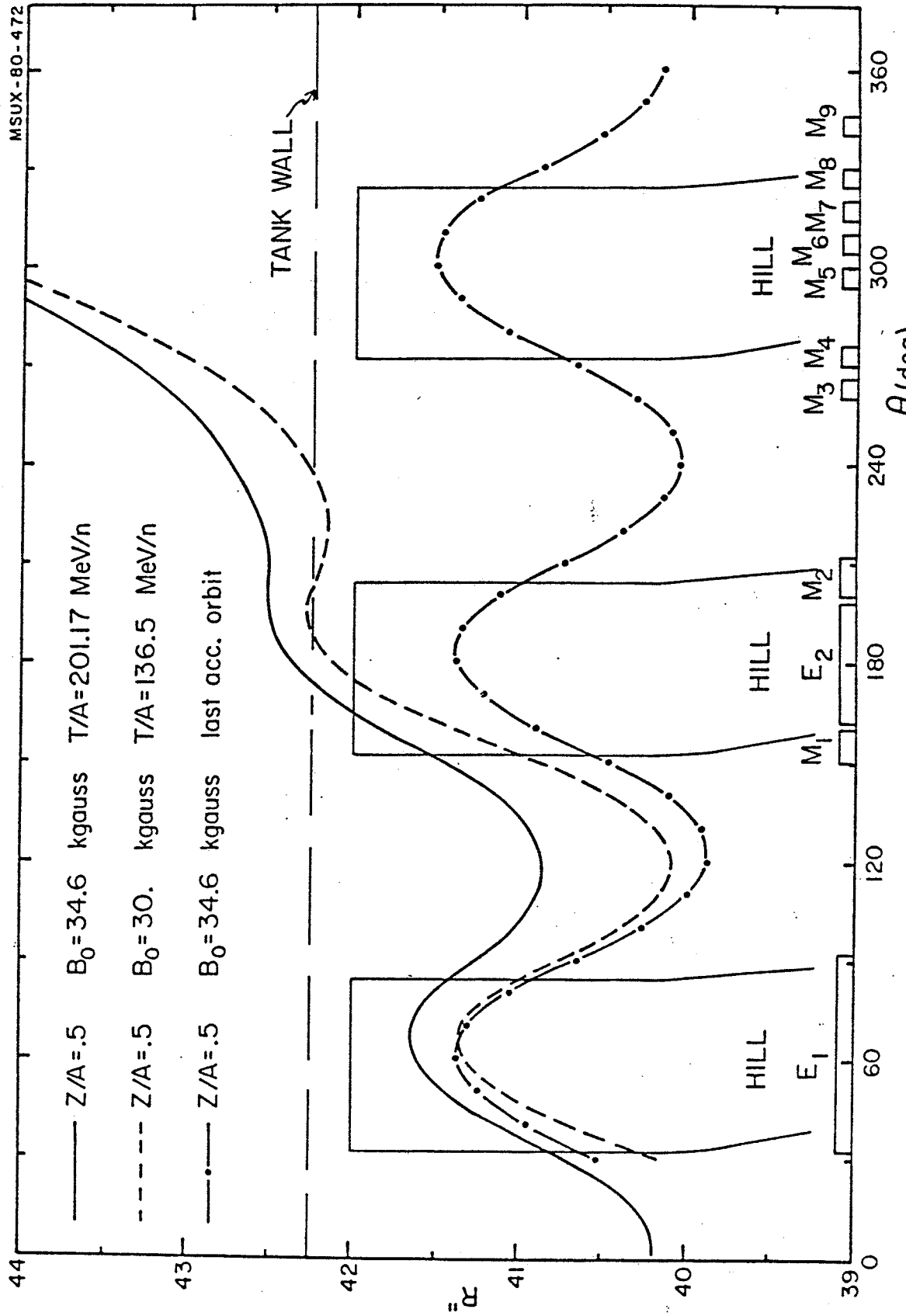

Fig. 46. Last accelerated orbit and extracted trajectories for two ions with Z/A = .5 and two different field values, in the (R,θ) plane.

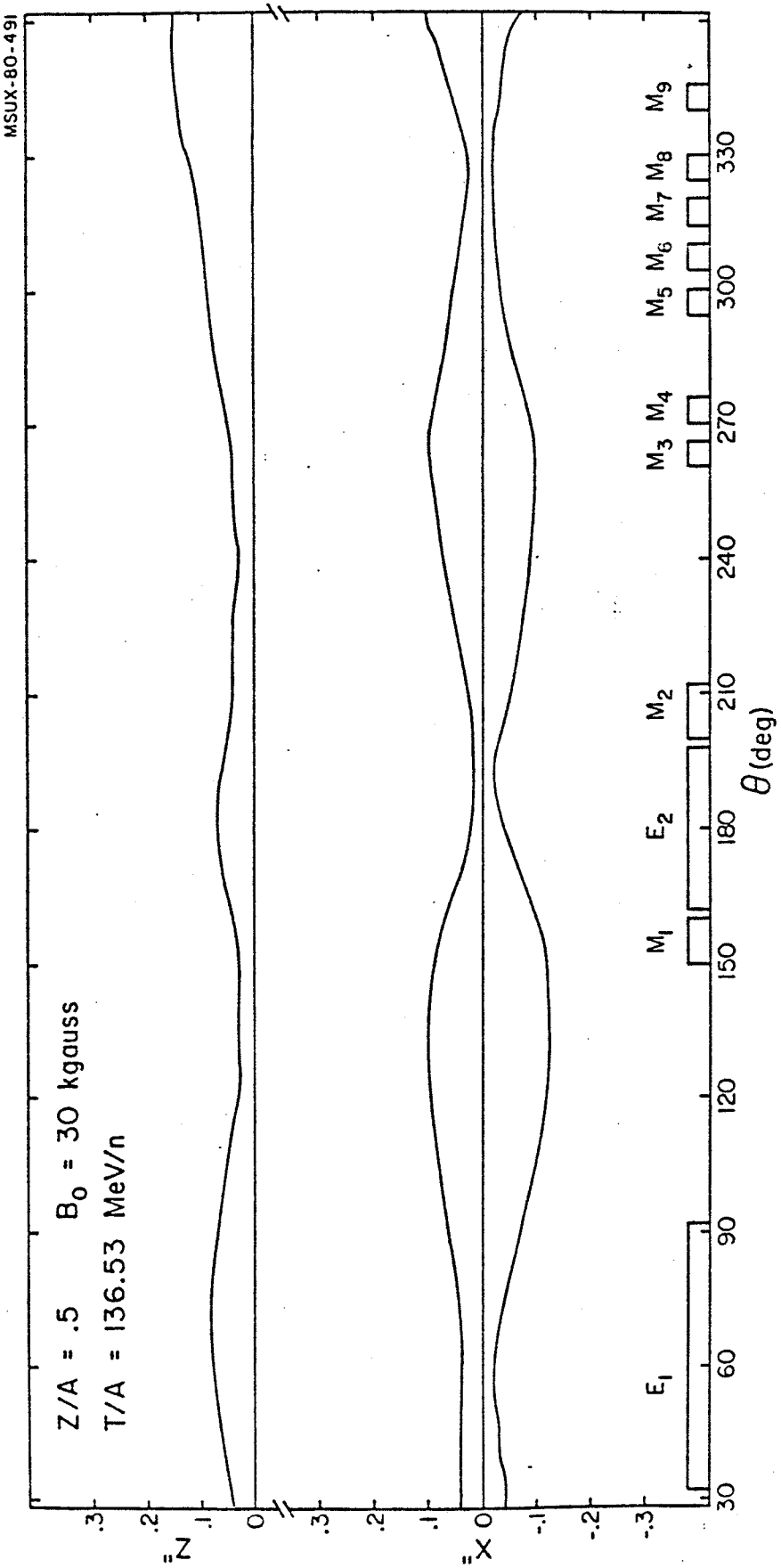

Fig. 48. Envelope, radial and axial, of an extracted beam of 136.5 MeV/n, traced through the extraction system.

is, however, of a few months at most.

In summary, therefore, the design of the K800 discussed here seems totally adequate to guarantee the anticipated machine performances.